# AN EXPERIMENTAL INVESTIGATION ON AXIAL AND CIRCUMFERENTIAL EFFECTS OF FLOW OBSTACLES ON SINGLE PHASE HEAT TRANSFER

A. Tanase<sup>1</sup>, D.C. Groeneveld<sup>1</sup>, H.Zahlan<sup>1</sup>

<sup>1</sup>University of Ottawa, Ontario, Canada

#### **Abstract**

The paper presents and discusses the experimental results obtained for various geometries and flow parameters (such as the obstruction ratio, obstacle shape, Re number) that may impact the single phase heat transfer in tubes equipped with flow obstacles. A review of previous work and current experimental data suggest that the main enhancement mechanisms are disruption of viscous boundary layer, enhancement of turbulent mixing and fin effect. The enhancement effects were observed up to 50 diameters downstream of a flow obstacle. Comparisons of the measured heat transfer enhancement with existing and a newly proposed prediction methods are presented.

#### Introduction

Convective heat transfer is the dominant heat transfer mechanism within the vast majority of heat transfer systems in fossil-fuelled and nuclear power plants. Previous experimental studies and numerical simulations have indicated that, in general, flow obstacles act as turbulence promoters and improve the downstream heat transfer coefficient, although at the expense of increased pressure drop. Proper design and optimization of heat transfer systems (including fuel bundles) equipped with turbulence promoters requires an understanding of the complex mechanisms that govern the flow patterns, pressure drop and heat transfer around flow obstructions.

It is expected that a more accurate prediction of enhancement effect provided by the flow obstacles allows an accurate determination of the Onset of Nucleate Boiling (ONB) boundaries, a more accurate prediction of the maximum sheath temperature during reactor accident conditions and a more reliable method for validating numerical simulation tools and models.

Few investigators have examined the effect of flow blockages on heat transfer in the turbulent flow region. Those who did, usually employed a rod bundle geometry equipped with grid spacers, examined the obstacle effect during film-boiling heat transfer instead of single-phase heat transfer or studied the hydrodynamic and heat transfer at relatively low flows, with little practical interest. The main objectives of the proposed investigation are:

- (i) To provide an experimental data base for heat transfer enhancement in single phase turbulent flow downstream of flow obstacles for various shapes.
- (ii) Improve our understanding of the physics of heat transfer enhancement caused by flow obstacles.

(iii) Derive an improved prediction methodology for heat transfer enhancement near obstacles, capable of accounting for various geometric and flow effects that have not been considered previously.

#### 1. Literature review

Most experiments examining the effect of flow obstacles on heat transfer have been performed on bundle geometries, e.g. Yao et al., (1982), Rehme (1977), Kidd and Hoffman (1968), Hassan and Rehme, (1981).

Yao, S.C. et al. (1982) performed a study of heat transfer enhancement in rod bundles near grid spacers, for single phase and post critical-heat-flux flow regimes. It was observed that the Nusselt number reaches a maximum at, or slightly behind the flow obstacle. After the fluid leaves the spacer, the hydrodynamic and thermal boundary layers begin to re-establish their fully developed profiles. The boundary layer phenomenon is similar to the entry length effect of turbulent tube flow. According to the authors, the main mechanism of heat transfer augmentation at spacer location is flow acceleration due to flow area contraction. For relatively large obstacles, the fin effect cooling (i.e. conduction effect) can be another effective cooling mechanism. In the wake region, the heat transfer is enhanced by the turbulent wakes created downstream of an obstacle as flow decelerates.

Downstream of obstacle the augmentation of heat transfer has been observed to be an exponentially decaying function of z/D where z is the distance downstream of the blockage:

$$\frac{Nu}{Nu_0} = 1 + 5.55\varepsilon^2 \exp\left(-0.13\frac{z}{D}\right) \tag{1}$$

where  $Nu_0$  is Nusselt number of the bare tube and Nu refers the tube equipped with flow obstacles. The authors recommends Equation (1) for Reynolds number higher than  $10^4$ .

The exponentially decaying trend has been matched reasonably well by the predictions. Similar results were obtained by Hassan and Rehme (1981), who performed tests with air in a three-rod subassembly, equipped with honeycomb-type spacer grids. Three sizes of the spacers were used, obstructing the flow by 25.3%, 30.2% and 34.8%. The Reynolds number was varied between 600 and  $2 \cdot 10^5$ , to simulate gas-cooled reactor conditions. They found a significant improvement in heat transfer by the spacer grid. In particular: (i) the highest increase (from 50% to 100%) was observed at the downstream end of the grid, and this improvement decayed exponentially with distance downstream from the obstacle, (ii) grids with the largest flow obstruction area resulted in the highest heat transfer enhancement, and (iii) with increasing Reynolds number the improvement decreased, and the axial extent of the influence was reduced. Hassan and Rehme (1981) also developed and recommended a correlation accounting for the spacer grid effect on heat transfer.

An experimental investigation conducted by Yao et al (1995) used two methods of flow visualization - hydrogen bubble and dye injection- to study the vortex dynamics and heat transfer enhancement mechanisms in the presence of flow obstacles. The obstacle, located in a rectangular channel, was prismatic with square cross section, with an estimated obstruction ratio of 20%; flow Re number was 10,500. The experiment revealed that the Karman vortices are shed from the wake of the obstacle, with a velocity close to the mainstream velocity and they tend to move in a criss-cross motion along the channel. The paper concluded that the "washing" action exerted by discrete vortices islands is the main mechanism of heat transfer enhancement.

The experimental results of Doerffer et al (1996) showed that for an obstacle with obstruction ratio of 17.8% (defined as the ratio of cross section of the obstacle and the cross section of a bare tube) the maximum heat transfer augmentation (versus the bare tube) occurred just downstream of the obstacle and was 38% for Re=3.9·10<sup>4</sup> and decreased to 14% for Re=2.3·10<sup>5</sup>. For the annular obstacle having 30% obstruction ratio, the heat transfer enhancement was 61% in the low Re range (3.9·10<sup>4</sup>) and 34% at higher Re numbers (2.3·10<sup>5</sup>). The enhancement effect decreased exponentially with distance downstream from the obstacle. It has been found that, for the obstacle having the lowest obstruction ratio, the effect was significant up to 5 diameters (z/D=5) downstream and for the highest obstruction ratio the effect extended to about 15 diameters. The authors explained the enhancement effect of the obstacle by two mechanisms: flow acceleration at the obstruction plane and increased turbulent mixing downstream the obstacle. The work confirmed the previous findings that for the same obstruction ratio, the highest heat transfer enhancement is observed at lower Re numbers and decreases as flow Re number increases.

Holloway et al. (2004) measured the circumferentially averaged heat transfer coefficient downstream of support grids, with and without flow-enhancing features, at Re numbers between 28,000 and 42,000. The geometrical configurations consisted 5x5 square array rod bundle with support grids, disk blockages and split vanes, respectively. Data analysis suggested that both power-law or exponential functions can reasonably describe the decay of enhancement effect with distance downstream from the obstacle. The authors proposed several semi-empirical correlations for heat transfer enhancement downstream of spacers with or without flow enhancing features. The heat transfer enhancement downstream of a standard support grid (without flow enhancing features) is described by the Equation (2):

$$\frac{Nu}{Nu_0} = 1 + 6.5\varepsilon^2 \exp(-0.8z/D)$$
 (2)

The same experimental data were also correlated in the power-law form and the following equation resulted:

$$\frac{Nu}{Nu_0} = 1 + 3.0\varepsilon^2 \left(\frac{z}{D_h}\right)^{-1.3} \tag{3}$$

The data base for these correlations covered a z/D range of 1.4 - 33.6.

In addition to the previous work (Holloway, 2004) which studied mainly the effects of axial distance downstream of flow obstacles, Holloway et al. (2005) also studied the circumferential variation of heat transfer coefficient in rod bundles. The circumferential variations were measured for three specific support grid designs (standard grid, split-vane pair grid and disc grid) at axial locations between 2.2 to 36.7 hydraulic diameters downstream from the grid, at Re numbers of 28,000 and 42,000, respectively. The geometrical setup consisted of a 5x5 square array rod bundle. The experimental results indicated that the highest circumferential variation of Nu number occurred just downstream (at z/D =2.2) of the grid and decreased with the development of the flow downstream. The circumferential variations for disc type obstacle were very small and within the experimental measurement accuracy. By contrast, much larger variations (+30% to -15%) were observed for split-vane pair. The axial distance after which the circumferential effect vanished was between 25 to 35 hydraulic diameters.

# 2. Experiment

# 2.1 Experimental loop

The 14<sup>th</sup> International Topical Meeting on Nuclear Reactor Thermalhydraulics, NURETH-14 Toronto, Ontario, Canada, September 25-30, 2011

The experiment was conducted in the multi-fluid test loop at University of Ottawa using HFC-134a as working fluid. The main components of the loop are test section, condenser, pressurizer, pumps, preheaters, power supply and loop instrumentation. (see Figure 1). The test section is directly heated by a 12 kW DC power supply (40V, 300 A). The inlet and outlet fluid temperatures of the test section are measured by two resistance temperature detectors (RTDs). The flow is recirculated by two gear pumps, installed in series, and delivering a constant volumetric flow rate.



1-gear pump, 2-Coriollis type mass-flow-meter, 3-pre-heater, 4-dielectric fittings, 5-power terminals, 6-electrical pre-heater, 7-sight glass, 8-condenser, 9-pressurizer, 10-pressure relief valve, 11-refrigerant filter-dryer, 12-ball-valve, 13-vacuum pump, 14-refrigerant storage tank, 15-pressure reducer, 16-nitrogen container.

#### Figure 1 Experimental Multi-Fluid Loop (Vertical Test Section).

A bypass around the pumps controls the flow rate. The flow is measured by a Coriollis flow meter with an accuracy of better than 0.5% (flow range 0-0.34 kg s<sup>-1</sup>). The pressure in the loop is controlled by the pressurizer, containing a heating coil at the bottom and a cooling coil near the top. The power to the pressurizer heater (maximum 500 W) is regulated by an adjustable AC transformer. An electric pre-heater (maximum power 5 kW) and a coaxial heat exchanger (with hot water on the secondary side) are located between the pumps and the test section. They are used to adjust the test section inlet fluid temperature or inlet mass quality to the desired values. The vapour generated in the test section is condensed by a coaxial heat exchanger prior to the fluid being recirculated to the pump. A piezoelectric pressure sensor measures the absolute pressure at the outlet of the test section (TS), and a differential pressure sensor measures the pressure drop along the TS.

#### 2.2 Test section

The experiments were performed in an electrically heated flow tube, made of Inconel 600 and having an inside diameter (ID) of 5.46 mm, an outside diameter (OD) of 8.00 mm, a total length of 2 m and a

heated length of 0.9 m. The exterior wall temperature of the test section was measured by six K-type self-adhesive thermocouples, located in pairs 180° apart at three planes. Three types of flow obstacles were inserted sequentially in the test section: a blunt cylinder, a rounded cylinder and an annular cylinder, coaxial with the test section. Each obstacle has a length of 10 mm and they were all manufactured from mild steel (see Figure 2). A ceramic magnet, located on the outside of the test section, held the obstacle at the desired location.

#### 2.3 Test matrix

The axial effect of flow obstacles was measured at z = 3, 5, 7, 10, 20, 30, 50 and 70 test section diameters (ID) downstream from the flow obstacles. Two obstacle shapes (streamlined and blunt), two obstruction ratios (15% and 30%) four mass fluxes and six heat fluxes were investigated. Test matrices are shown in Table 1, for geometry and in Table 2, for flow parameters.

Table 1 Experimental test matrix for geometrical parameters

Obstruction ratio (%)	Shape	Relative distance downstream of trailing edge (z/D)
15, 30	A(annular obstruction) B (blunt cylinder) R (rounded cylinder)	3, 5, 7, 10, 20, 30, 50, 70

Table 2 Experimental test matrix for flow parameters

Mass flux (kg m <sup>-2</sup> s <sup>-1</sup> )	Heat flux (kWm <sup>-2</sup> )	
500	20, 30	
1000	30, 65	
2000	65, 120	
3500	120, 200	

#### 3. Results and discussion

#### 3.1 Parametric trends

The existing prediction methods (Equations 1, 2 and 3) relate heat transfer enhancement to obstruction ratio ( $\epsilon$ ) and the dimensionless distance downstream of a flow obstacle (z/D) Although this captures two important parameters that impact heat transfer enhancement, it does not take into account all potentially significant factors. The experimental data indicate that enhancement of convective heat transfer coefficient downstream of a flow obstacle is also influenced by the obstacle

The 14<sup>th</sup> International Topical Meeting on Nuclear Reactor Thermalhydraulics, NURETH-14 Toronto, Ontario, Canada, September 25-30, 2011

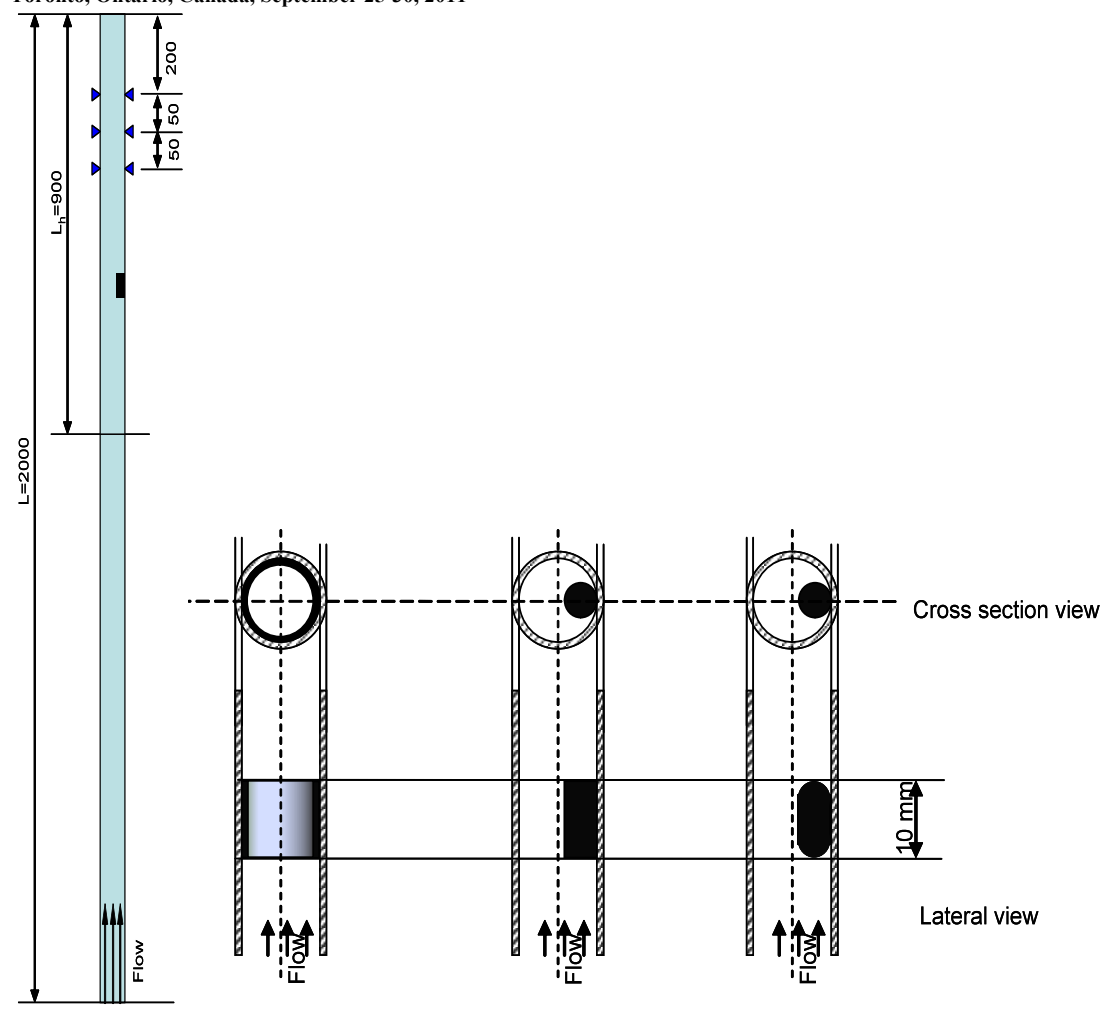


Figure 2 The schematic of test section, thermocouples layout and the obstacle types (from left to right: annular, blunt and rounded)

shape, Reynolds number (Re) and circumferential location of the obstacle. A discussion of the parameters that affect the heat transfer enhancement downstream a flow obstacle is provided below:

Obstruction ratio: The obstruction ratio significantly influences the enhancement ratio (the ratio between the Nusselt number for the obstacle-equipped tube and the Nusselt number for the bare tube) downstream a flow obstacle. Figures 5 – 8 show that for the entire range of flow Reynolds numbers, an increase of the obstruction ratio from 15% to 30%, leads to significant increase of heat transfer enhancement. For example, an increase of the obstruction ratio from 15% to 30% resulted to an increase of the enhancement ratio from 1.35 to 1.7 at Re=14,500 and from 1.13 to 1.34 at Re=100,000, respectively. (values at z/D=3 for the rounded obstacle).

<u>Distance downstream from the obstacle:</u> It has been reported (Yao et al.,1982, , Holloway et al., 2004) the enhancement effect decreases exponentially with the dimensionless distance (z/D) downstream from an obstacle. However, different authors disagree on the distance after which the obstacle effect vanishes. It has been suggested by Yao et al. (1982) that the obstacle effect is similar to the entrance effect in a turbulent channel. Incropera et al. (2007), describing the entrance effect, suggested that single phase internal turbulent flow needs between 10 and 60 diameters to reach fully developed velocity profile; for the same effect Miheev (1968) recommended 50 hydraulic diameters. Doerfer et al (1996) indicated that the enhancement effect lasted up to 15 z/D downstream the

obstacle. Figures 5 to 8 indicate that the obstacle effect is still measurable up to z/D=50 for the blunt and rounded obstacles, but, by contrast the effect of the annular obstacle disappears at z/D=30.

Obstacle shape: The obstacle shape has a minimal impact in the lower Re range, but it increases as Re number increase. At lower Re number turbulent flow, blunt obstacles produce slightly higher enhancement, followed closely by the rounded and the annular obstacles, respectively; this trend is observed for both 15% and 30% obstruction ratios. However, in the higher Re number range (Re>50,000), noticeable differences between obstacles having different shapes but the same obstruction ratio are observed. The experiments indicate that in this flow range, the rounded obstacle provided the highest heat transfer enhancement; the smallest enhancement was observed for the annular obstacle.

Reynolds number: The impact of flow Re number is generally significant; the experimental data show that the enhancement ratio decreases as Re number increases. This observation applies to all obstacle shapes and obstruction ratios investigated. For example, for the 30% rounded obstacle, the maximum enhancement ratio decreases from 1.7 at Re = 14,500 to 1.35 at Re = 100,000. For 15% blunt obstacle, it decreases from 1.33 at Re = 14,500 to 1.13at Re = 100,000. A similar trend of heat transfer enhancement versus Re number has been reported for the entrance effect of turbulent flow in tubes (Miheev, 1968).

<u>Circumferential location</u>: The measurement of circumferential distribution of heat transfer coefficient downstream of an obstacle indicated that, overall, the heat transfer coefficient increases more on the side of the wall closest to the obstacle. A typical circumferential effect is presented in Figure 7.

The circumferential distribution of heat transfer enhancement is relatively smooth for the obstacles with low obstruction ratios; however, blunt obstacle with high obstruction ratios show a more irregular distribution. Another important observation is that on the heated wall located opposite to an obstacle, a lower heat transfer coefficient (versus the bare tube values) may be observed. This heat transfer reduction has been noted for the obstacles with low obstruction ratios. We believe that the diminished heat transfer coefficient is caused mainly by diversion of bulk flow towards the wall closest to the obstacle, thus increasing the heat transfer on that side, but decreasing the flow velocity (thus the local heat transfer coefficient) on the opposite side. This explanation is supported by measurements of circumferential distribution of heat transfer coefficient (see Figure 7), as well as by flow visualizations (see Figure 9).

#### 3.2 Enhancement mechanisms

Osthuizen (2007) pointed out that that, unlike laminar flow, the velocity profile of fully developed turbulent flow can not be predicted through a fully theoretical approach, but rather using semi-empirical means. Three main regions have been identified (see Figure 10):

- viscous sublayer represents the region very close to the wall; within this region, the molecular viscosity effects are important. The velocity profile is linear; momentum and heat transfer are governed by molecular diffusion (i.e. thermal conduction for heat transfer), thus relatively large velocity and temperature gradients are typical; Slanciaukas (2001) reported that the main resistance to turbulent-flow heat transfer for most common liquids (such as water, glycerol, oil) is in the viscous sublayer. As an example, it is mentioned that for a fluid with Prandtl (Pr) number equal to 5, it causes about 60% of temperature drop between the heated surface and the bulk fluid temperatures. However, it is worth mentioning that as the Pr number decreases, the proportion of temperature drop in the viscous sublayer decreases, as well.
- *turbulent core* denotes the region far from the wall; within this region, the molecular viscosity effects are negligible. Heat and momentum transfer are controlled by turbulent mixing. Because turbulent mixing is a very effective heat and mass transfer mechanism, the velocity and temperature gradients are small.

• intermediate region or *buffer layer*, represents the transition region between the viscous sublayer and the turbulent core; the molecular and turbulent properties are comparable, thus none of them can be neglected.

A literature review and analysis of experimental data suggested three heat transfer enhancement mechanisms associated with flow obstacles:

# 1) Disruption of boundary layer

It can be assumed that, when a fluid impinges an obstacle with height larger than the viscous sublayer thickness, the viscous sublayer at the location of the obstacle is disrupted. As previously mentioned, through the viscous sublayer the heat transfer is governed by thermal conduction, which is less effective than concurrent heat transfer mechanisms (e.g. advection); removal or disruption of the "insulating" viscous sublayer significantly enhances the local heat transfer rate. This mechanism is effective for the obstacles larger than the thickness of viscous sublayer. If the obstacle does not occupy the whole circumference of the heated wall (such as an eccentrically located obstacle), the viscous sublayer thickness in the flow area is expected to decrease. The main reason is the flow area contraction that results in increased flow velocity. Some researchers (Yao et al. 1982) suggested that the redevelopment of boundary layer is similar to the entrance effect in a heated channel. This similarity is based on the assumption that in both cases the viscous boundary layer develops and it needs a certain distance to reach its fully developed profile. According to Miheev (1968), the entrance effect in heated tubes lasts for about 50 hydraulic diameters, for  $10^4 < Re < 10^6$ . This assumption is supported by current experimental data (see Figures 5 to 8).

# 2) <u>Increase of turbulent mixing</u>

Qualitative experimental observations (see Figure 11) and previous research work (Yao et al., 1995, Doerfer et al., 1996) indicate that around and downstream of a flow obstruction, a system of steady and unsteady coherent structures (eddies) are formed. Depending on the flow Reynolds number, large unsteady eddies travel downstream, break down and transfer their mass and energy to smaller eddies, and this process continues until the smallest eddies are dissipated by molecular viscosity. All these processes are known as the energy cascade and are very effective in transferring momentum and energy within the fluid. Furthermore, the interaction between larger eddies and the viscous boundary layer may disrupt the latter thus enhancing heat transfer (Yao et al., 1995). Of a particular interest is the reattachment area downstream of a flow obstacle (i.e. the region behind the steady recirculating wake vortex, where the main flow impinges the heated wall). Several authors (Terekhov et al, 2002) indicate that that this area represents a local maximum of heat transfer enhancement. Some of the plots at Re >50,000 (Figures 7 and 8) seem to support this hypothesis.

#### 3) Fin effect

This mechanism is effective for relatively large obstacles with high thermal conductivity and good thermal contact with the heated wall. Due to its pure conductive nature, the area of influence is limited around the obstacle and depends on the material properties and the geometry of the heated tube and the flow obstacle.

#### 3.3 Prediction methods

A comparison between the current and newly proposed prediction methods against the current experimental data has been performed (see Table 3). Several statistical parameters have been used, namely the average of errors and root mean square of errors. Relative error is defined as the

difference between the predicted 
$$\left(\frac{Nu}{Nu_0}\right)_{predicted}$$
 and measured enhancement  $\left(\frac{Nu}{Nu_0}\right)_{measured}$  ratios

divided by the measured enhancement ratio.

The average and root mean square (RMS) of errors are computed as:

$$Avg = \frac{\sum_{i=1}^{N} error_{i}}{N}$$

$$RMS = \sqrt{\frac{\sum_{i=1}^{N} error_{i}^{2}}{N-1}}$$
(4)

Table 3 Comparison between prediction methods and current experimental data

Prediction method	Average of errors (%)	RMS of errors (%)
Yao et al. (1982)	-3.59	4.73
Holloway et al. (2004)	-9.31	9.40

A comparison between our experimental data (averaged circumferentially) and the existing prediction methods - Yao et al (1982) and Holloway (2004) - reveals significant differences. Both prediction methods tend to under predict the experimental data, especially at low Re numbers, Re< 35,000. However, at Re > 50,000, the correlation of Yao et al. (1982) shows better agreement with the experimental data. Note that the error in predicting the heat transfer enhancement ([Nu-Nu<sub>0</sub>]/Nu) is much larger as can be seen in Figures 3 and 4.

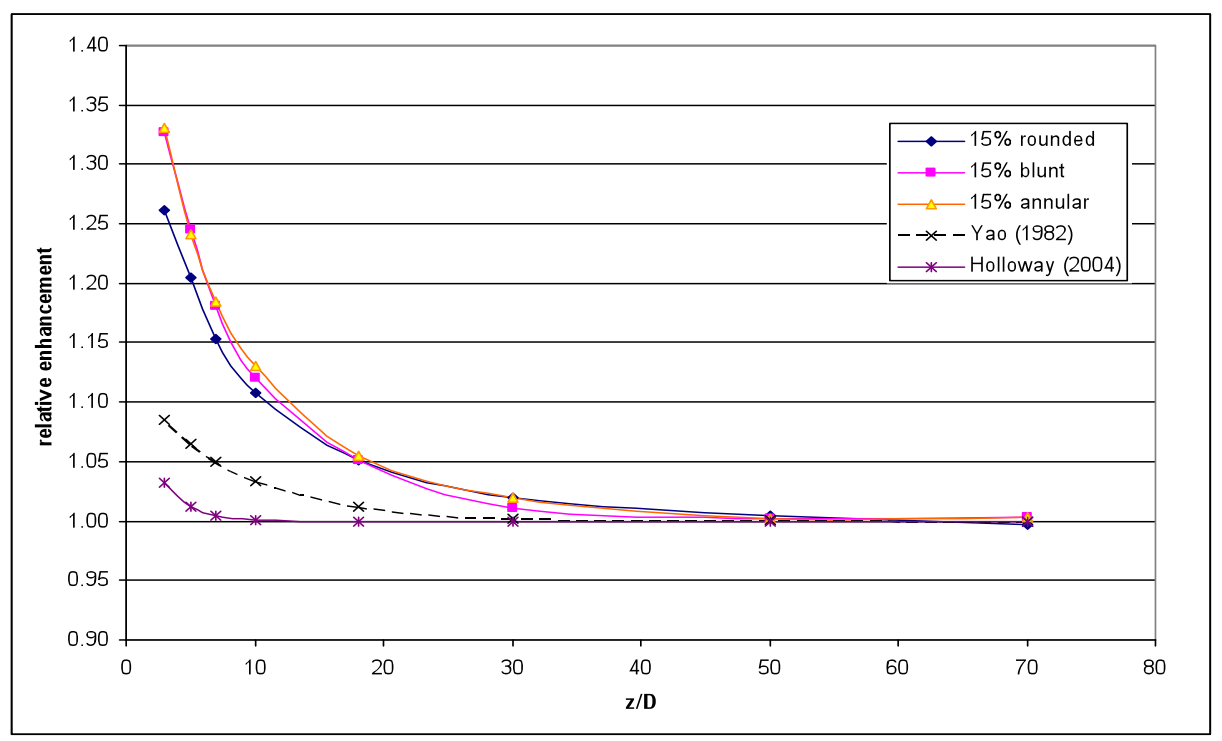


Figure 3 Comparison of Yao (1982) and Holloway(2004) prediction methods with experimental data at Re=14,500, for obstacles with 15% obstruction ratio

The 14<sup>th</sup> International Topical Meeting on Nuclear Reactor Thermalhydraulics, NURETH-14 Toronto, Ontario, Canada, September 25-30, 2011

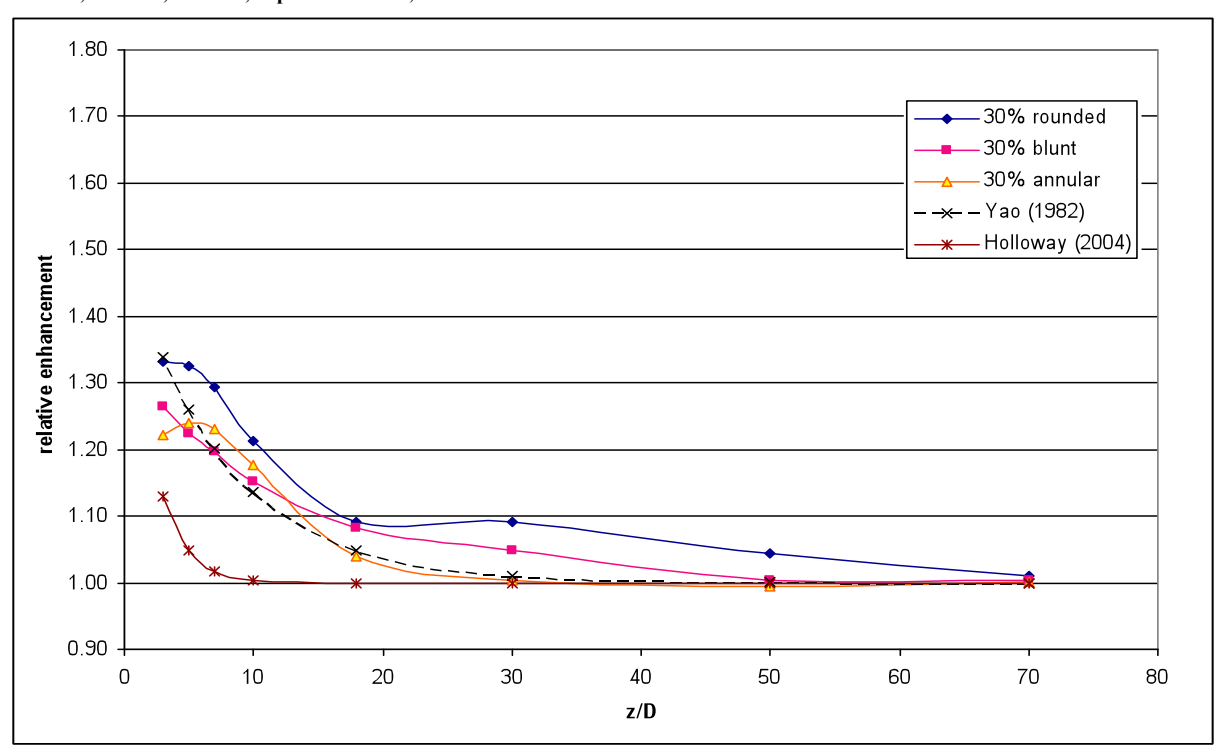


Figure 4 Comparison of Yao (1982) and Holloway(2004) prediction methods with experimental data at Re=100,000 for obstacles with 30% obstruction ratio

In order to derive an improved prediction method, the following assumptions were made:

- the enhancement decays exponentially with distance downstream of an obstacle;
- three obstructions ratios were considered 0%, 15% and 30%; 0% was selected in order to ensure correct asymptotic trends (that is, no enhancement for 0% obstruction ratios);
- the enhancement is dependent on the obstruction ratio ( $\epsilon$ ), dimensionless distance downstream from an obstacle (z/D) and the flow Re number (Re);

The correlation of the current experimental data resulted in the following expressions:

$$\frac{Nu}{Nu_0} = 1 + Ae^{-B\frac{z}{D_h}}$$

$$A = 23640 \,\text{Re}^{-0.9627} \,\varepsilon e^{(1.236 \,\ln(\text{Re}) - 10.73)\varepsilon}$$

$$B = 0.4613 - 0.0343 \,\ln(\text{Re})$$
(5)

The proposed prediction method predicts the data with an average error of -0.2% and an RMS error of 2.49%. The prediction accuracy of existing and the proposed prediction methods differ significantly. The difference can be explained by the geometrical setup (tube versus bundle geometries) and by the number of flow and geometrical parameters considered (three versus two parameters). The comparison suggests that the prediction methods derived from fuel bundle data should be cautiously applied to other flow geometries. The comparison between prediction methods revealed that the existing methods tend to underpredict the current experimental data, especially in the lower flow range. Relatively large difference between Yao and Holloway prediction methods indicates that they are primarily suitable for the geometries and flow conditions used for their derivation. Although the new proposed correlation does not accounts for all parameters of interest (such as circumferential location or obstacle shape) or fin effect, it is more elaborated than the existing prediction methods and considers more flow parameters.

#### 4. Conclusions

The experimental investigation suggested that the following parameters influence of the enhancement of forced convective heat transfer downstream of a flow obstacle:

- Obstruction ratio of the obstacle
- Dimensionless distance downstream from the obstacle (z/D)
- Obstacle shape
- Flow Reynolds number
- Circumferential location of the obstacle (for eccentric geometries)

A tentative improved prediction method which takes into account the obstruction ratio, dimensionless distance downstream from the obstacle and the flow Reynolds number has been developed; it provides satisfactory accuracy for the range of data investigated and correct parametric trends for the present test geometry. Further improvements may involve consideration of other parameters of interest, such as the obstacle shape, circumferential position of the obstacle and test geometry.

The experimental data indicated that, for the flow Re up to 50,000, for a given obstruction ratio, the heat transfer enhancements given by obstacles of various shapes were comparable; however, in the higher Re number range (100,000>Re>50,000) the rounded shaped obstacle produced noticeably higher enhancement. This effect was observed for both -15% and 30% - obstruction ratios.

The circumferential position of an eccentrically located obstacle with 15% obstruction ratio appears to impact the circumferential distribution of heat transfer coefficient up to 30 to 50 diameters downstream from the flow obstacle; the same effect was observed, albeit to a lesser extent, for the obstacles with 30% obstruction ratio.

A literature review and analysis of experimental data suggested three heat transfer enhancement mechanisms associated with flow obstructions: i) disruption of boundary layer and ii) increase of turbulent mixing and, iii) fin effect. Their relative importance may vary according to the flow geometry and Re number. However, more investigations (experiments or numerical simulations) should be conducted to confirm and further clarify the heat transfer enhancement mechanisms.

Prediction methods derived from experimental data obtained for fuel bundles should be cautiously applied to other flow geometries. A statistical analysis of various prediction methods suggested that the existing methods tend to underpredict current experimental data, especially in the lower flow range.

It is recognized that the enhancement of heat transfer coefficient downstream of a flow obstruction is obtained at the expense of increased pressure drop, thus the effective use of flow obstructions require a complex optimization process(e.g. shape, obstruction ratio, pitch, position in the channel). It is suggested that future work in this area to address the pressure drop and the complex relationship between pressure drop and the heat transfer enhancement.

#### 5. References

- [1] Doerffer, S., D.C. Groeneveld and J.R. Schenk, (1996), Experimental Study of the Effects of Flow Inserts on Heat Transfer and Critical Heat Flux, *Proceedings of the 4th Int. Conference on Nuclear Engineering, vol. 1 Part A, pp.41-49, March 10-14, New Orleans, Louisiana, USA*
- [2] Hassan, M.A., Rehme, K.,(1981), Heat transfer near spacer grids in gas-cooled rod bundles, *Nucl. Technol. Vol. 52*, 410–414

- [3] Holloway, M.V., McClusky, H.L., Beasley, D.E. and Conner, M.E., (2004), The effect of support grid features on local, single-phase heat transfer measurements in rod bundles, *Journal of Heat Transfer, Vol. 124*
- [4] Holloway, M., Conover, T., McClusky, H., Beasley, D. and Conner, M.E. (2005), The effect of support grid design on azimuthal variation in heat transfer coefficient for rod bundles, *Journal of Heat Transfer, Vol. 127*
- [5] Incropera, F.P. and DeWitt, D.P., (2007), Fundamentals of Heat and Mass Transfer, Sixth edition, John Wiley & Sons
- [6] Miheev, M.A. Fundamentals of Heat Transfer, (1968), Mir, Moscow
- [7] Rehme, K. (1977), Pressure drop of spacer grids in smooth and roughened rod bundles, *Nuclear Technology, Vol. 33*
- [8] Slanciaukas, A (2001) Two friendly rules for the turbulent heat transfer enhancement, *Int. Journal of Heat and Mass Transfer*, (44), 2155-2161
- [9] Terekhov, V.I., Yarygina, N.I., Zhdanov, R.F. (2002), Some features of a turbulent separated flow and heat transfer behind a step and a rib, *Journal of Applied Mechanics and technical Physics*, Vol.43, No.6, 888-894
- [10] Yao, M, Nakatani, M and Suzuki, K. (1995), Flow visualization and heat transfer experiments in a turbulent channel flow obstructed with an inserted square rod, *Int. J Heat and Fluid Flow* 16, 389-397
- [11] Yao, S.C., Hochreiter, W.J. and Leech, W.J. (1982), Heat transfer augmentation in rod bundles near grid spacers, *Transactions of the ASME*, Vol. 104, 76-81
- [12] Osthuizen, P.H and Naylor, D. (2007), An Introduction to Single Phase Convective Heat Transfer Analysis, *William C Brown Pub*

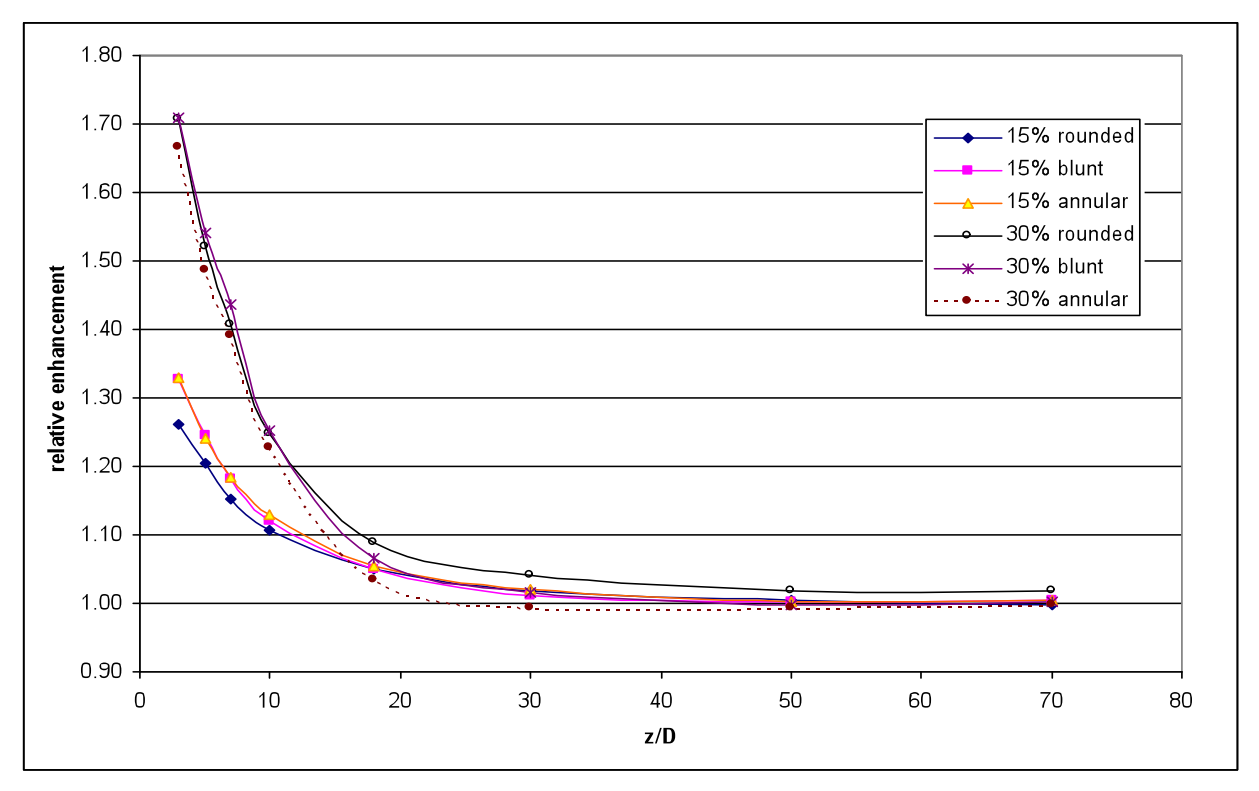


Figure 5 Comparison of relative enhancement between various obstacle types at  $G=500 \text{ kg m}^{-2}\text{s}^{-1}$ , Re =1.45·10<sup>4</sup>

The 14<sup>th</sup> International Topical Meeting on Nuclear Reactor Thermalhydraulics, NURETH-14 Toronto, Ontario, Canada, September 25-30, 2011

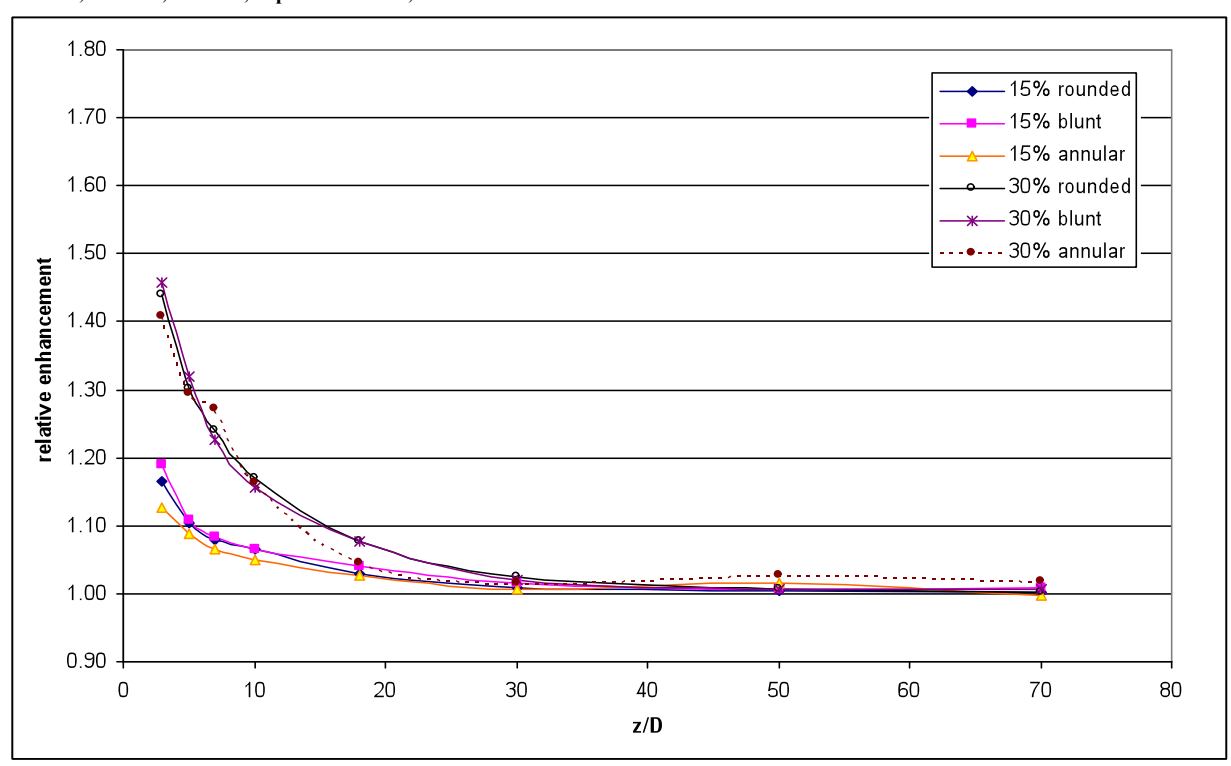


Figure 6 Comparison of relative enhancement between various obstacle types at  $G=1000~kg~m^{-2}s^{-1}$ , Re =2.8·10<sup>4</sup>

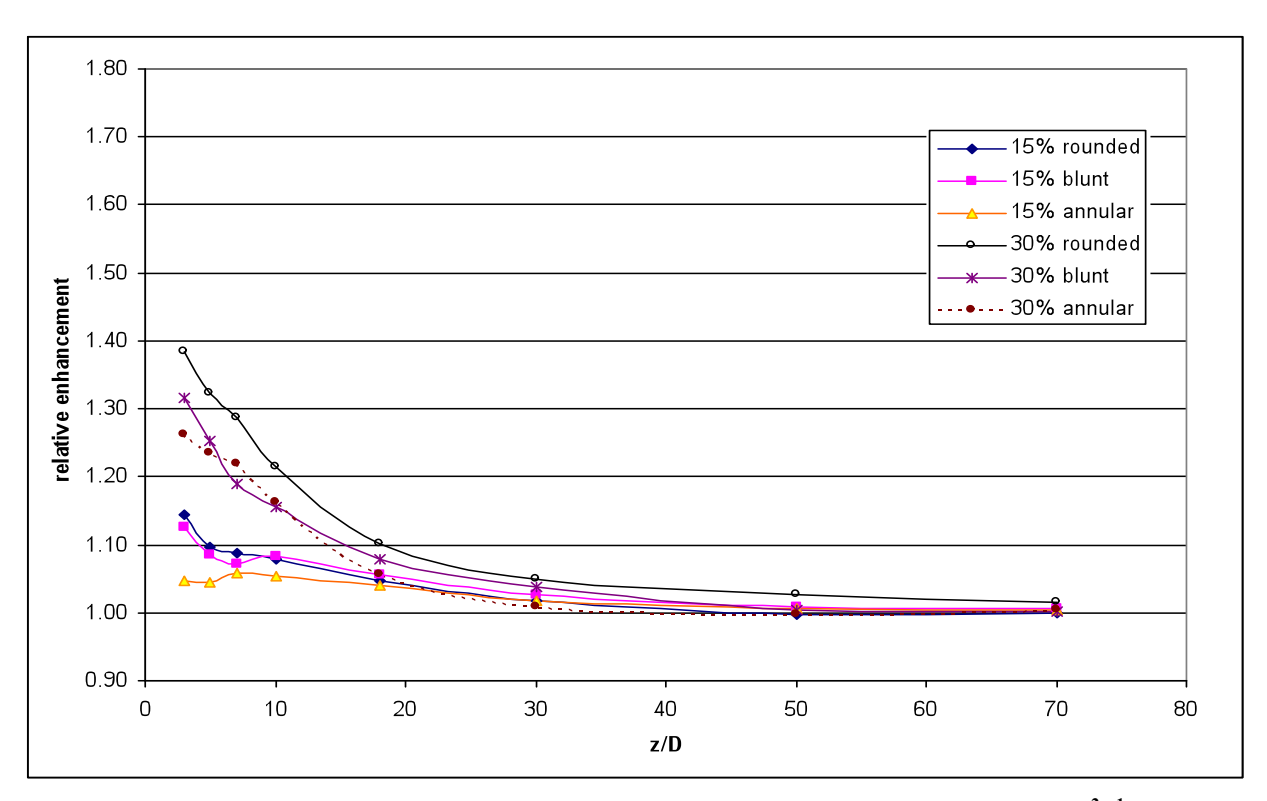


Figure 7 Comparison of relative enhancement between various obstacle types at  $G=2000 \text{ kg m}^{-2}\text{s}^{-1}$ , Re =5.5·10<sup>4</sup>

The 14<sup>th</sup> International Topical Meeting on Nuclear Reactor Thermalhydraulics, NURETH-14 Toronto, Ontario, Canada, September 25-30, 2011

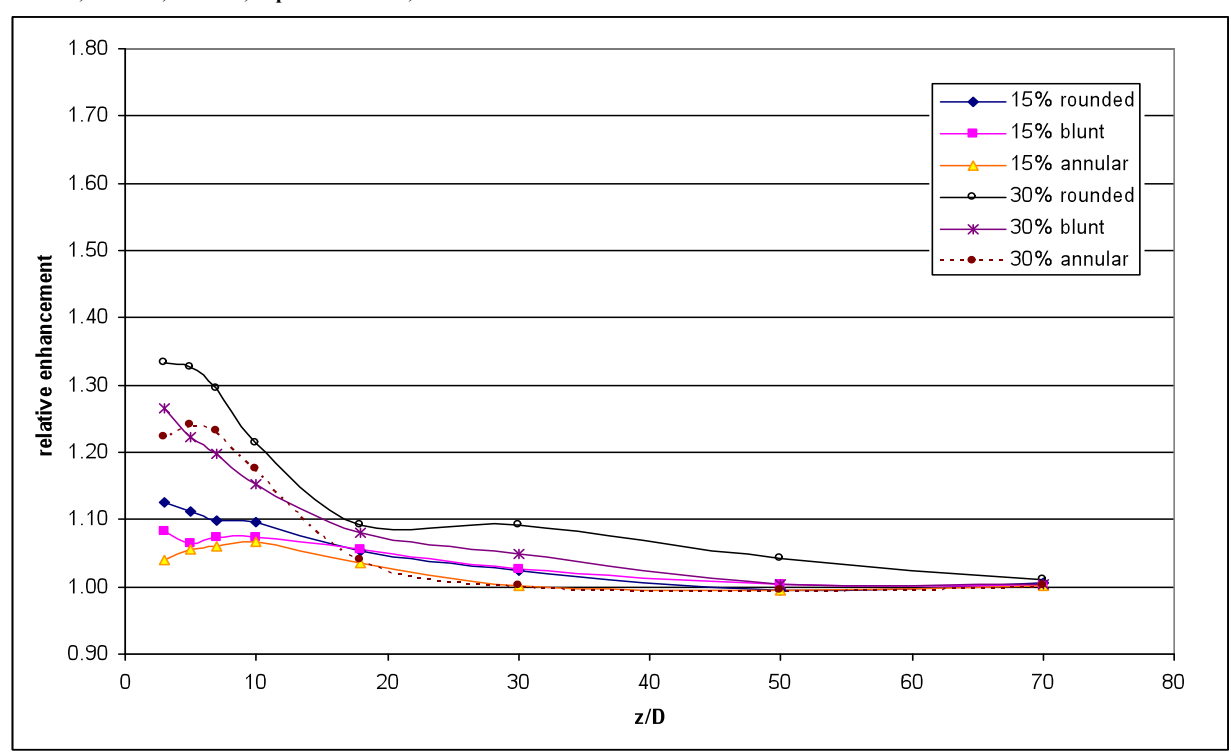


Figure 8 Comparison of relative enhancement between various obstacle types at G=3500 kg m  $^{\text{-}2}\text{s}^{\text{-}1},$  Re =1.0·10 $^{\text{-}5}$ 

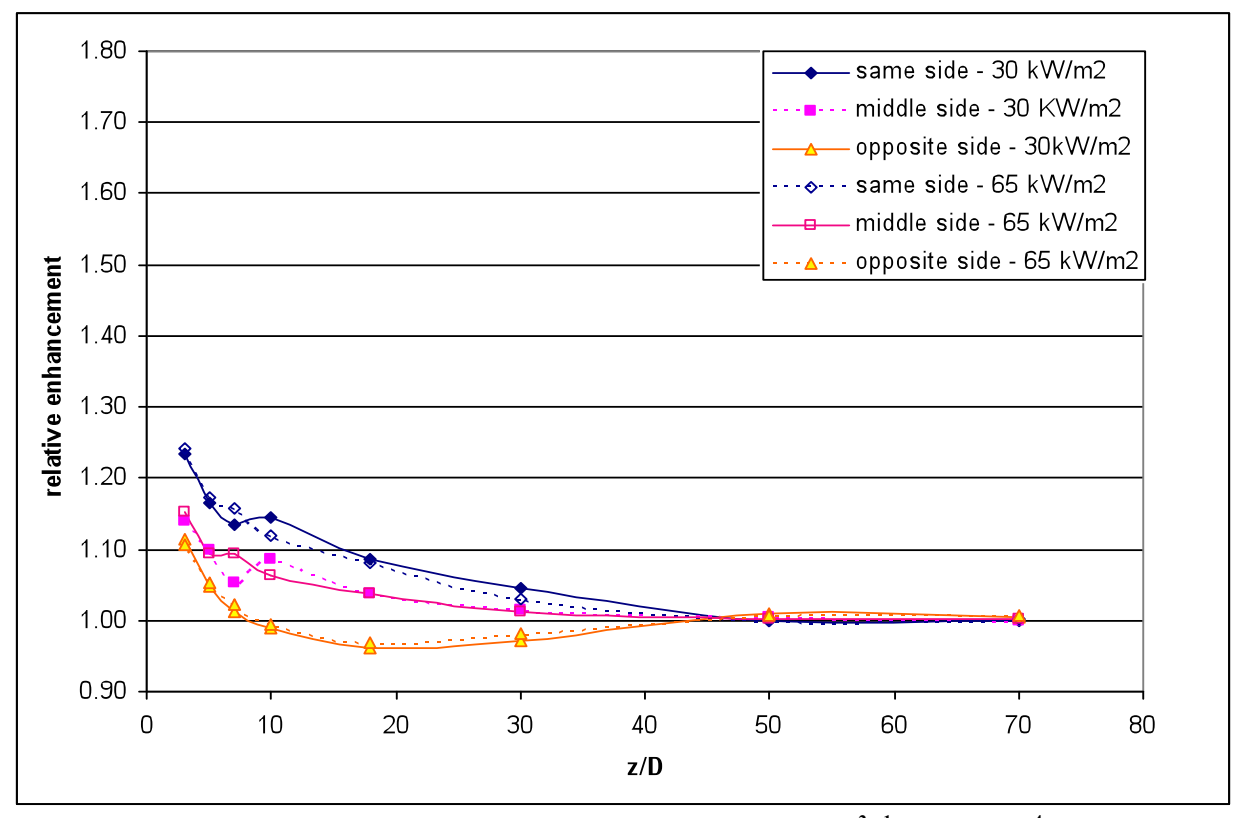


Figure 9 Circumferential effect for 15% rounded obstacle at G=1000 kg m<sup>-2</sup>s<sup>-1</sup>, Re =2.8·10<sup>4</sup>

The 14<sup>th</sup> International Topical Meeting on Nuclear Reactor Thermalhydraulics, NURETH-14 Toronto, Ontario, Canada, September 25-30, 2011

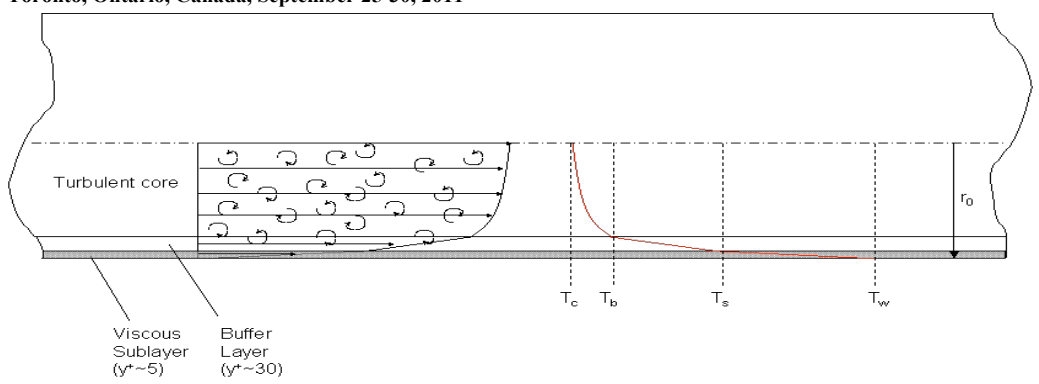


Figure 10 Typical velocity and temperature variation (heated wall) in a longitudinal cross section in fully developed turbulent pipe flow

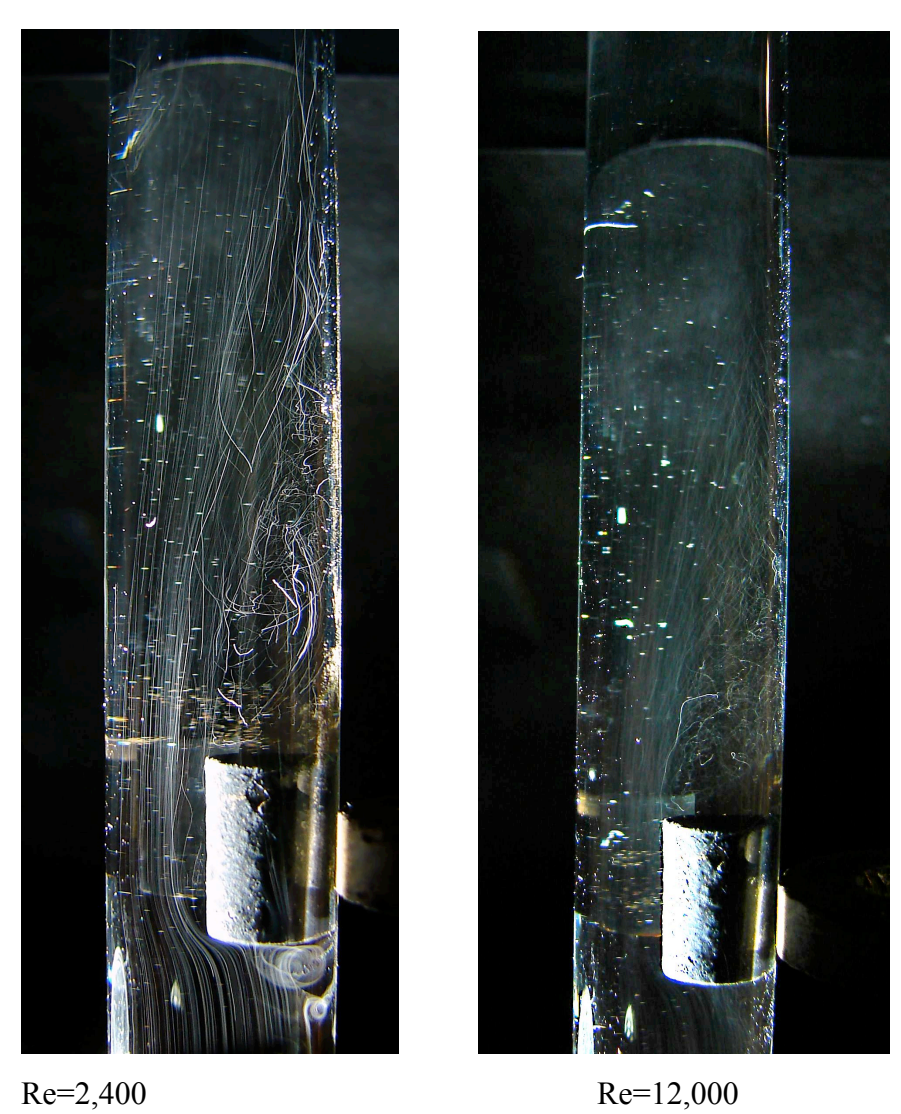


Figure 11 Hydrogen bubbles flow visualization around 30% blunt obstacle in laminar (Re=2,400) and turbulent (Re=12,000) flow